AIAA JOURNAL
Vol. 49, No. 4, April 2011

Nonlinear Mode Interaction for Thin Circular Cylindrical Anisotropic Shells

Ronald P. Notenboom*
Netherlands Defense Academy, 1780 CA Den Helder, The Netherlands
and
Johann Arbocz†
Delft University of Technology, 2629 HS Delft, The Netherlands

DOI: 10.2514/1.J050465

The Sanders shell equations for imperfect anisotropic circular cylindrical shells are used for the development of a research tool to study the nonlinear interaction of circumferential waves under different loading conditions. Therefore, a truncated Fourier series in circumferential direction is used as a possible solution of the nonlinear equilibrium equations in combination with the anisotropic constitutive relations. The envelope of the Fourier series coefficients in the axial direction is computed using a numerical integration technique satisfying the rigorous boundary conditions at the lower and upper shell edges. The case of an isotropic shell under axial compression is used to compare the results obtained by the current theory and the STAGS-A program.

Nomenclature

$[\boldsymbol{A}]$	=	shell wall extensional stiffness matrix
$[\boldsymbol{B}]$	=	shell wall coupling stiffness matrix
$[\boldsymbol{D}]$	=	shell wall bending stiffness matrix
$\bar{E}$	=	Young's modulus, reference value
$[\boldsymbol{E}]$	=	modified stiffness matrix
$[\boldsymbol{F}]$	=	modified stiffness matrix
$[\boldsymbol{G}]$	=	modified stiffness matrix
K	=	modified stress resultant
$K^{(x)}$	=	external edge load at x
L	=	shell length
M_x	=	stress resultant (moment)
M_y	=	stress resultant (moment)
M_{xy}	=	stress resultant (moment)
M_1, M_2	=	applied bending moments
N	=	number of circumferential wave numbers
N_x	=	stress resultants (force)
N_y	=	stress resultants (force)
N_{xy}	=	stress resultants (force)
$N^{(x)}$	=	external edge load at x
$\mathbb{N}$	=	set of full circumferential wave numbers
n_k	=	full circumferential wave number
P	=	applied axial load
p_e	=	external pressure
Q_x	=	modified stress resultant
R	=	shell radius
S	=	shell middle surface
S_1, S_2	=	applied shear loads
T	=	applied torsional moment
t	=	shell wall thickness
U	=	strain energy
u	=	axial displacement
v	=	circumferential displacement
W	=	work done by external loads
w	=	radial displacement
w^*	=	initial imperfection
x, y, z	=	coordinate system
$\boldsymbol{Y}$	=	vector with primary variables
β_x, β_y	=	rotations
β_x^*, β_y^*	=	modified rotations
γ_{xy}	=	shear strain
$\varepsilon_x, \varepsilon_y$	=	membrane strains
$\varkappa_x, \varkappa_y, \varkappa_{xy}$	=	curvatures
λ	=	load factor
$\bar{\nu}$	=	Poisson's ratio reference value
Π	=	total potential energy
ρ_{xy}	=	modified curvature
σ_x, σ_y	=	normal stresses
τ_{xy}	=	shear stresses

Introduction

RECENTLY a shell design approach was proposed by Arbocz et al. [1,2] called "high-fidelity analysis," where the uncertainties involved in a design are simulated by refined and more accurate numerical methods. This hierarchical analysis includes three levels of analysis: 1) classical solution with simply supported boundary conditions and linear membrane prebuckling; 2) including the effect of nonlinear prebuckling and clamped or simply supported boundary conditions; and 3) including nonlinear interaction between nearly simultaneous buckling modes, midsurface and boundary imperfections and general boundary conditions. The Delft Interactive Shell DEsign COde (DISDECO) program is based on the preceding approach and developed at the Delft University of Technology.

The DISDECO level 2 module COLLAPSE [3] based on the Donnell type shell equations is not always accurate, especially in the case of isotropic shells, since the response model contains only one wave number in the circumferential direction. A new level 2, nonlinear mode interaction module called Thin Anisotropic SHell Analysis (TASHA) is developed, based on Sanders' shell theory [4], in combination with anisotropic shell wall material. The approximate solution of the nonlinear equations is a truncated Fourier series in circumferential direction and in the axial direction the governing differential equations are solved using numerical integration techniques. The theory and results are compared with results obtained by the finite difference program STAGS-A [5].

Received 8 February 2010; revision received 11 November 2010; accepted for publication 3 December 2010.

*Assistant Professor, NLDA-KIM Military Sciences, PO Box 10000; rp.notenboom@nlda.nl.

†Professor (Emeritus), Aerospace Engineering, Kluyverweg 1; j.arbocz@tudelft.nl. Fellow AIAA.

Shell Geometry and Axis System

The geometry and the axis system used for the analysis of the thin circular cylindrical shell with small initial imperfections, are shown in Fig. 1. The radius of the shell middle surface is R, the wall thickness is t and the shell length is L. The right-handed-axis system is chosen such that the axial coordinate x runs from the lower to the upper edge, the circumferential coordinate y runs counterclockwise, and the positive z-axis is taken inward. The known small initial imperfection $w^*(x, y)$ is also taken positive inward.

Kinematic Relations

The analysis uses the Sanders type of nonlinear kinematic relations for thin circular cylindrical shells with small initial imperfections, given by [4,6]

$$\varepsilon_x = u_{,x} + \frac{1}{2}\beta_x^2 - \beta_x w^*_{,x} \tag{1}$$

$$\varepsilon_y = v_{,y} - \frac{1}{R}w + \frac{1}{2}\beta_y^2 - \beta_y w^*_{,y} \tag{2}$$

$$\gamma_{xy} = v_{,x} + u_{,y} + \beta_x\beta_y - \beta_x w^*_{,y} - \beta_y w^*_{,x} \tag{3}$$

$$\varkappa_x = \beta_{x,x} \tag{4}$$

$$\varkappa_y = \beta_{y,y} \tag{5}$$

$$\varkappa_{xy} = \beta_{x,y} + \beta_{y,x} \tag{6}$$

where the rotations are

$$\beta_x = -w_{,x} \qquad \beta_y = -w_{,y} - \frac{1}{R}v \tag{7}$$

Stress Resultants and Constitutive Relations

The shell wall is in a state of plane stress, see Fig. 2. In order to obtain the stress resultants the stresses are integrated over the wall thickness t. For thin walls, i.e., $t/R \ll 1$, the stress resultants are

$$\begin{pmatrix} N_x \\ N_y \\ N_{xy} \end{pmatrix} = \int_{z=-t/2}^{t/2} \begin{pmatrix} \sigma_x \\ \sigma_y \\ \tau_{xy} \end{pmatrix} \mathrm{d}z \tag{8}$$

$$\begin{pmatrix} M_x \\ M_y \\ M_{xy} \end{pmatrix} = \int_{z=-t/2}^{t/2} z \begin{pmatrix} \sigma_x \\ \sigma_y \\ \tau_{xy} \end{pmatrix} \mathrm{d}z \tag{9}$$

Since $\tau_{xy} = \tau_{yx}$, the stress resultants $N_{xy} = N_{yx}$ and $M_{xy} = M_{yx}$. The stress resultants are shown in Fig. 3.

The constitutive relations for an anisotropic shell wall are given by the relations

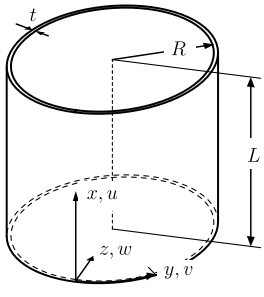

Fig. 1 Shell geometry and axis system.

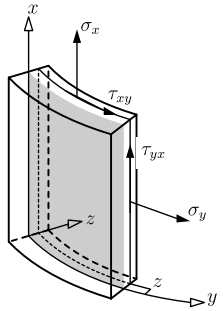

Fig. 2 Stresses on a plane with radius ($R - z$).

$$\boldsymbol{N} = [\boldsymbol{A}]\boldsymbol{\varepsilon} + [\boldsymbol{B}]\boldsymbol{\kappa} \tag{10}$$

$$\boldsymbol{M} = [\boldsymbol{B}]\boldsymbol{\varepsilon} + [\boldsymbol{D}]\boldsymbol{\kappa} \tag{11}$$

where $[\boldsymbol{A}]$ is the extensional stiffness matrix, $[\boldsymbol{B}]$ the coupling stiffness matrix and $[\boldsymbol{D}]$ the bending stiffness matrix. Further,

$$\boldsymbol{N} = (N_x \quad N_y \quad N_{xy})^T, \qquad \boldsymbol{M} = (M_x \quad M_y \quad M_{xy})^T$$

and

$$\boldsymbol{\varepsilon} = (\varepsilon_x \quad \varepsilon_y \quad \gamma_{xy})^T, \qquad = (\varkappa_x \quad \varkappa_y \quad \varkappa_{xy})^T$$

Equilibrium Equations

The equilibrium equations for the circular cylindrical shell with small initial imperfections can be derived from the condition of stationary potential energy. The total potential energy Π is given by

$$\Pi = U - W \tag{12}$$

where U is the strain energy and W the work done by the external loads:

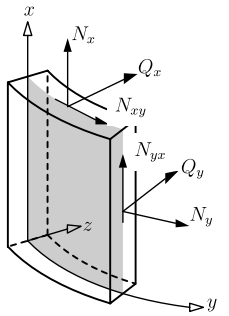

a) Forces on shell middle surface

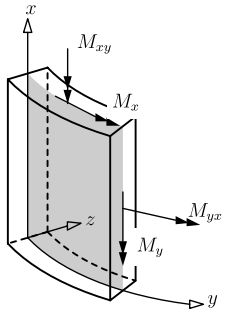

b) Moments on shell middle surface

Fig. 3 Stress resultants on the shell middle plane.

$$U = \frac{1}{2}\iint_S (\boldsymbol{N}^T\boldsymbol{\varepsilon} + \boldsymbol{M}^T\boldsymbol{\kappa})\,\mathrm{d}S \tag{13}$$

where S is the shell middle surface.

The following external loads are considered: external pressure p_e, axial load P, bending moments M_1 and M_2, torsional moment T and shear loads S_1 and S_2. The external loads on the upper edge are shown in Fig. 4. These loads can be applied using the following equations for the distributed loads, shown in Fig. 5:

$$\begin{aligned} N^{(L)}(\theta) &= \frac{P}{2\pi R} + \frac{M_1}{\pi R^2}\cos\theta + \frac{M_2}{\pi R^2}\sin\theta \\ K^{(L)}(\theta) &= \frac{T}{2\pi R^2} + \frac{S_1}{\pi R}\cos\theta + \frac{S_2}{\pi R}\sin\theta \end{aligned} \tag{14}$$

The work done by the external loads is given by

$$\begin{aligned} W = &\int_{\theta=0}^{2\pi} [u\langle N^{(L)}\rangle + v\langle K^{(L)}\rangle]_{x=L} R\,\mathrm{d}\theta - \int_{\theta=0}^{2\pi} [u\langle N^{(0)}\rangle \\ &+ v\langle K^{(0)}\rangle]_{x=0} R\,\mathrm{d}\theta + \iint_S w p_e\,\mathrm{d}S \end{aligned} \tag{15}$$

The equilibrium conditions imply $\delta\Pi = \delta U - \delta W = 0$, yielding the following equilibrium equations:

$$N_{x,x} = -N_{xy,y} \tag{16}$$

$$K_{,x} = -N_{y,y} - \frac{1}{R}M_{y,y} - \frac{1}{R}(N_y\beta_y^* + N_{xy}\beta_x^*) \tag{17}$$

$$Q_{x,x} = -\frac{1}{R}N_y - M_{y,yy} + [N_y\beta_y^* + N_{xy}\beta_x^*]_{,y} - p_e \tag{18}$$

$$M_{x,x} = -Q_x + (N_x\beta_x^* + N_{xy}\beta_y^*) \tag{19}$$

where K is given by

$$K = N_{xy} - \frac{1}{R}M_{xy} \tag{20}$$

and

$$\beta_x^* = \beta_x - w_{,x}^* \tag{21}$$

$$\beta_y^* = -w_{,y} - \frac{1}{R}v - w_{,y}^* \tag{22}$$

The condition $\delta\Pi = 0$ also determines the boundary conditions on the shell edges $x = 0$ and $x = L$:

$$\int_{y=0}^{2\pi R} [\delta u\langle N_x - N^{(x)}\rangle]_x\,\mathrm{d}y = 0 \tag{23}$$

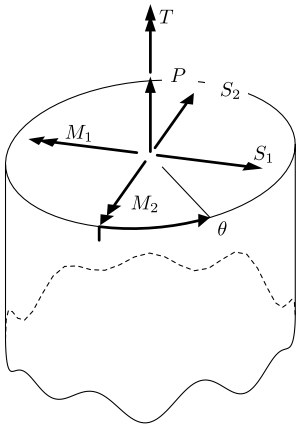

Fig. 4 External load on upper edge ($x = L$).

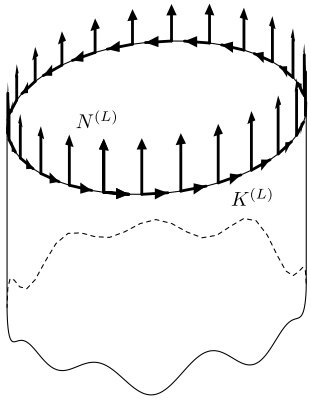

Fig. 5 Distributed loads $N^{(L)}$ and $K^{(L)}$ on upper edge ($x = L$).

$$\int_{y=0}^{2\pi R} [\delta v\langle K - K^{(x)}\rangle]_x\,\mathrm{d}y = 0 \tag{24}$$

$$\int_{y=0}^{2\pi R} [\delta w\langle Q_x\rangle]_x\,\mathrm{d}y = 0 \tag{25}$$

$$\int_{y=0}^{2\pi R} [\delta\beta_x\langle M_x\rangle]_x\,\mathrm{d}y = 0 \tag{26}$$

Using Eqs. (23–26) the classical boundary conditions are defined, shown in Table 1.

Separation of Variables

To be able to use the method of separation of variables, the constitutive relations Eqs. (10) and (11) are reordered into the following form:

$$\begin{pmatrix} N_x \\ M_x \\ K \end{pmatrix} = [\boldsymbol{G}]\begin{pmatrix} \varepsilon_x \\ \kappa_x \\ \gamma_{xy} \end{pmatrix} + [\boldsymbol{F}]\begin{pmatrix} \varepsilon_y \\ \kappa_y \\ \rho_{xy} \end{pmatrix} \tag{27}$$

$$\begin{pmatrix} N_y \\ M_y \\ M_{xy} \end{pmatrix} = [\boldsymbol{F}^T]\begin{pmatrix} \varepsilon_x \\ \kappa_x \\ \gamma_{xy} \end{pmatrix} + [\boldsymbol{E}]\begin{pmatrix} \varepsilon_y \\ \kappa_y \\ \rho_{xy} \end{pmatrix} \tag{28}$$

where the new variable ρ_{xy} is defined as

$$\rho_{xy} = \kappa_{xy} + \frac{1}{R}\gamma_{xy} \tag{29}$$

The three matrices $[\boldsymbol{G}]$, $[\boldsymbol{F}]$ and $[\boldsymbol{E}]$ contain appropriate elements from the stiffness matrices $[\boldsymbol{A}]$, $[\boldsymbol{B}]$ and $[\boldsymbol{D}]$.

From Eq. (27), the following relation is found:

$$\begin{pmatrix} \varepsilon_x \\ \kappa_x \\ \gamma_{xy} \end{pmatrix} = [\boldsymbol{G}^*]\begin{pmatrix} N_x \\ M_x \\ K \end{pmatrix} - [\boldsymbol{F}^*]\begin{pmatrix} \varepsilon_y \\ \kappa_y \\ \rho_{xy} \end{pmatrix} \tag{30}$$

Substitution of Eq. (30) into Eq. (28) yields

$$\begin{pmatrix} N_y \\ M_y \\ M_{xy} \end{pmatrix} = [\boldsymbol{F}^{*T}]\begin{pmatrix} N_x \\ M_x \\ K \end{pmatrix} + [\boldsymbol{E}^*]\begin{pmatrix} \varepsilon_y \\ \kappa_y \\ \rho_{xy} \end{pmatrix} \tag{31}$$

where

$$[\boldsymbol{G}^*] = [\boldsymbol{G}^{-1}] \tag{32}$$

$$[\boldsymbol{F}^*] = [\boldsymbol{G}^{-1}\boldsymbol{F}] \tag{33}$$

and

Table 1 Prescribed variables for the classical boundary conditions on thin cylindrical shells

Boundary type	Boundary condition	Boundary condition	Boundary condition
SS-1	u	v	$w = M_x = 0$
SS-2	N_x	v	$w = M_x = 0$
SS-3	u	K	$w = M_x = 0$
SS-4	N_x	K	$w = M_x = 0$
C-1	u	v	$w = \beta_x = 0$
C-2	N_x	v	$w = \beta_x = 0$
C-3	u	K	$w = \beta_x = 0$
C-4	N_x	K	$w = \beta_x = 0$
Free edge	N_x	K	$Q_x = M_x = 0$

$$[\boldsymbol{E}^*] = [\boldsymbol{E} - \boldsymbol{F}^T\boldsymbol{G}^{-1}\boldsymbol{F}] \tag{34}$$

Further, it holds that

$$\begin{pmatrix} \varepsilon_y \\ \varkappa_y \\ \rho_{xy} \end{pmatrix} = \begin{pmatrix} v_{,y} - \frac{1}{R}w + \frac{1}{2}\beta_y^2 \\ \beta_{y,y} \\ 2\beta_{x,y} + \frac{1}{R}(u_{,y} + \beta_x\beta_y) \end{pmatrix} + \begin{pmatrix} -\beta_y w^*_{,y} \\ 0 \\ -\frac{1}{R}(\beta_x w^*_{,y} - \beta_y w^*_{,x}) \end{pmatrix} \tag{35}$$

Using the kinematic relations Eqs. (1), (3), and (4), the vector $(\varepsilon_x \quad \varkappa_x \quad \gamma_{xy})^T$, can be written as

$$\begin{pmatrix} \varepsilon_x \\ \varkappa_x \\ \gamma_{xy} \end{pmatrix} = \begin{pmatrix} u_{,x} \\ \beta_{x,x} \\ v_{,x} \end{pmatrix} + \begin{pmatrix} \frac{1}{2}\beta_x^2 - \beta_x w^*_{,x} \\ 0 \\ u_{,y} + \beta_x\beta_y - \beta_x w^*_{,y} - \beta_y w^*_{,x} \end{pmatrix} \tag{36}$$

Using Eqs. (30) and (36) yields the following derivatives with respect to the axial coordinate x:

$$\begin{pmatrix} u_{,x} \\ \beta_{x,x} \\ v_{,x} \end{pmatrix} = [\boldsymbol{G}^*]\begin{pmatrix} N_x \\ M_x \\ K \end{pmatrix} - [\boldsymbol{F}^*]\begin{pmatrix} \varepsilon_y \\ \varkappa_y \\ \rho_{xy} \end{pmatrix} - \begin{pmatrix} \frac{1}{2}\beta_x^2 - \beta_x w^*_{,x} \\ 0 \\ u_{,y} + \beta_x\beta_y - \beta_x w^*_{,y} - \beta_y w^*_{,x} \end{pmatrix} \tag{37}$$

and from Eq. (7),

$$w_{,x} = -\beta_x \tag{38}$$

The values ε_y, $\varkappa_y$ and ρ_{xy}, can be written as

$$\varepsilon_y = \left(v_{,y} - \frac{1}{R}w\right) + \left(w_{,y} + \frac{1}{R}v\right)\left(\frac{1}{2}w_{,y} + \frac{1}{2R}v + w^*_{,y}\right) \tag{39}$$

$$\varkappa_y = -w_{,yy} - \frac{1}{R}v_{,y} \tag{40}$$

$$\rho_{xy} = \left(2\beta_{x,y} + \frac{1}{R}u_{,y}\right) - \frac{1}{R}\left(w_{,y} + \frac{1}{R}v\right)(\beta_x - w^*_{,x}) - \frac{1}{R}\beta_x w^*_{,y} \tag{41}$$

These are all functions of the primary variable vector $\boldsymbol{Y}$ and the derivatives $\boldsymbol{Y}_{,y}$ and $\boldsymbol{Y}_{,yy}$, where

$$\boldsymbol{Y} = (u \quad v \quad w \quad \beta_x \quad N_x \quad K \quad Q_x \quad M_x)^T \tag{42}$$

Substitution of Eqs. (39–41) into Eqs. (30) and (31), yields that also the vectors $(\varepsilon_x \quad \varkappa_x \quad \gamma_{xy})^T$ and $(N_y \quad M_y \quad M_{xy})^T$ are functions of the primary variables and their derivatives with respect to y.

Using the relation $N_{xy} = K + (1/R)M_{xy}$, the equilibrium conditions Eqs. (16–19) can be written as

$$N_{x,x} = -K_{,y} - \frac{1}{R}M_{xy,y} \tag{43}$$

$$K_{,x} = -N_{y,y} + \frac{1}{R}M_{y,y} - \frac{1}{R}\left(N_y\beta^*_y + K\beta^*_x + \frac{1}{R}M_{xy}\beta^*_x\right) \tag{44}$$

$$Q_{x,x} = -\frac{1}{R}N_y - M_{y,yy} + \left[N_y\beta^*_y + K\beta^*_x + \frac{1}{R}M_{xy}\beta^*_x\right]_{,y} - p_e \tag{45}$$

$$M_{x,x} = Q_x - N_x\beta^*_x - K\beta^*_y - \frac{1}{R}M_{xy}\beta^*_y \tag{46}$$

Equations (43–46) together with Eqs. (37) and (38), form a set of eight nonlinear differential equations, which can be written in the following form:

$$\boldsymbol{Y}_{,x} = \mathcal{F}(\boldsymbol{Y} \quad \boldsymbol{Y}_{,y} \quad \boldsymbol{Y}_{,yy} \quad w^*_{,x} \quad w^*_{,y}) \tag{47}$$

Assuming that the imperfection $w^*(x, y)$ and its derivatives with respect to the x and y coordinates are known functions, the solution of the set of differential equations of the primary variables is a periodic series in circumferential direction with coefficients that are functions of the axial coordinate x only; therefore,

$$\boldsymbol{Y}(x, y) = \boldsymbol{Y}_0(x) + \sum_{k=1}^{\infty}\left(\boldsymbol{Y}_{ck}(x)\cos k\frac{y}{R} + \boldsymbol{Y}_{sk}(x)\sin k\frac{y}{R}\right) \tag{48}$$

where $\boldsymbol{Y}_0$ is the axisymmetric part of the solution and $\boldsymbol{Y}_{c,k}$ and $\boldsymbol{Y}_{s,k}$ are the coefficients corresponding to the kth circumferential full wave number.

Equation (47) can now be written as a set of ordinary first-order differential equations:

$$\frac{\mathrm{d}\mathbf{Y}}{\mathrm{d}x} = \mathcal{F}\left(\mathbf{Y} \quad \frac{\mathrm{d}\mathbf{Y}}{\mathrm{d}y} \quad \frac{\mathrm{d}^2\mathbf{Y}}{\mathrm{d}y^2} \quad \frac{\mathrm{d}w^*}{\mathrm{d}x} \quad \frac{\mathrm{d}w^*}{\mathrm{d}y}\right) \tag{49}$$

Approximate Solution

Using a subset of N circumferential wave numbers,

$$\mathbb{N} = \{n_1, n_2, \cdots, n_N\} \quad \text{with} \quad 0 < n_1 < n_2 < \cdots < n_N \tag{50}$$

the approximation of the solution is given by

$$\tilde{\boldsymbol{Y}}(x, y) = \tilde{\boldsymbol{Y}}_0(x) + \sum_{j=1}^{N}\left(\tilde{\boldsymbol{Y}}_{cj}(x)\cos n_j\frac{y}{R} + \tilde{\boldsymbol{Y}}_{sj}(x)\sin n_j\frac{y}{R}\right) \tag{51}$$

Substitution of the approximate solution into Eq. (49) and using the Galerkin technique yields a set of $8(1 + 2N)$ ordinary first-order differential equations.

The nonlinear terms in the differential equations cause mode coupling. The quadratic and cubic terms represent coupling between the circumferential wave numbers

$$|\pm n_k \pm n_l| \quad \text{and} \quad |\pm n_k \pm n_l \pm n_m| \tag{52}$$

In the approximate solution only the wave numbers that are element of the set $\mathbb{N}$ are preserved.

In general the boundary conditions, Eqs. (23–26), are of the type

$$\int_{y=0}^{2\pi R}[\delta\zeta\langle Z\rangle]_x\,\mathrm{d}y = 0 \tag{53}$$

with ζ and Z both truncated series of the same form as Eq. (51). Hence the boundary condition becomes

$$\left.\begin{array}{rcl} \delta\zeta_0(x)=0 & \text{or} & Z_0(x)=0 \\ \text{and for } j=1,\cdots,N & & \\ \delta\zeta_{c,j}(x)=0 & \text{or} & Z_{c,j}(x)=0 \\ \delta\zeta_{s,j}(x)=0 & \text{or} & Z_{s,j}(x)=0 \end{array}\right\} \tag{54}$$

Numerical Solution

With N circumferential full wave numbers in the set $\mathbb{N}$, the number of ordinary first-order nonlinear differential equations, given by Eq. (49), is equal to $16N + 8$. At the shell edges at $x = 0$ and $x = L$, the number of prescribed values at each end is $8N + 4$. This makes the problem is a standard two point boundary value problem with nonlinear differential equations. The numerical method used to solve the problem is known as the multiple or parallel shooting method [7]. The numerical integration routines are from the California Institute of Technology (Caltech) Willis Booth Computer Center. These differential equation routines use the Runge–Kutta–Gill method to compute starting values for an Adams–Moulton predictor-corrector method both with automatic step size control.

To avoid very large or very small numbers, the governing equations are made nondimensional. Using a reference Young's modulus $\bar{E}$ and Poisson's ratio $\bar{\nu}$, the classical buckling load for a cylindrical shell with radius R and wall thickness t is

$$N_{cl} = \frac{\bar{E}t^2}{cR} \quad \text{where } c = \sqrt{3(1-\bar{\nu}^2)} \tag{55}$$

Further the following nondimensional variables are defined:
coordinates

$$\bar{x} = x/R \tag{56}$$

$$\theta = y/R \tag{57}$$

stiffness matrices

$$[\bar{A}] = [A]/(\bar{E}t) \tag{58}$$

$$[\bar{B}] = [B]\Big/\left(\frac{\bar{E}t^2}{2c}\right) \tag{59}$$

$$[\bar{D}] = [D]\Big/\left(\frac{\bar{E}t^3}{4c^2}\right) \tag{60}$$

shell displacements

Table 2 Properties of Caltech A8 shell

Property	Variable	Value
Radius	R	4.0 in.
Length	L	8.0 in.
Wall thickness	t	0.00464 in.
Young's modulus	E	$15.20\,10^6$ psi
Poisson's ratio	ν	0.3
Shear modulus	G	$5.84614\,10^6$ psi
Reference value	$\bar{E}$	$15.20\,10^6$ psi
Reference value	$\bar{\nu}$	0.3
Classical buckling load	N_{cl}	49.5152 lb/in.

Table 3 Limit load factor by STAGS for A8 shell

Mesh size, axial by circumferential	Limit load factor λ_{lim}
161×181	0.3295
261×261	0.3192

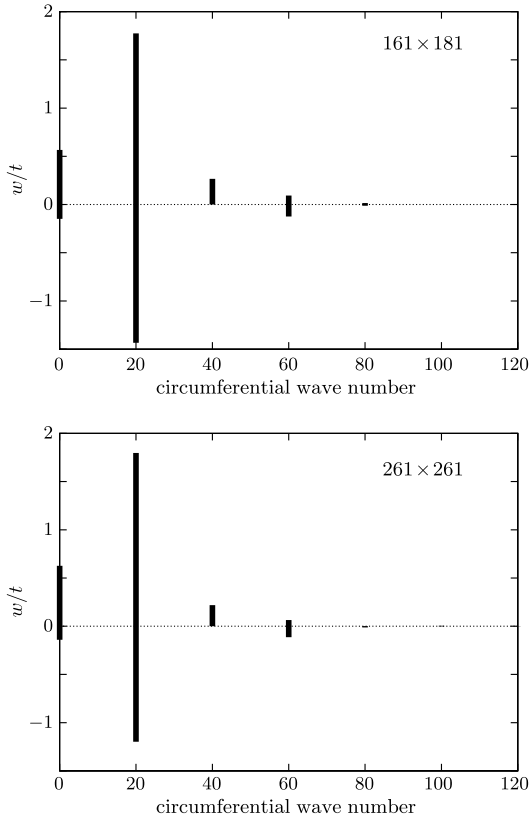

Fig. 6 Radial displacement coefficients $w_{c,\ell}$ extreme values at limit load, for two STAGS-A models.

$$\begin{pmatrix} \bar{u} \\ \bar{v} \\ \bar{w} \end{pmatrix} = \begin{pmatrix} u \\ v \\ w \end{pmatrix}\Big/ t \tag{61}$$

forces and moments per unit length

$$\begin{pmatrix} \bar{N}_x \\ \bar{K} \\ \bar{Q}_x \end{pmatrix} = \begin{pmatrix} N_x \\ K \\ Q_x \end{pmatrix}\Big/\left(\frac{\bar{E}t^2}{cR}\right) \tag{62}$$

$$\bar{M}_x = M_x\Big/\left(\frac{\bar{E}t^3}{2c^2R}\right) \tag{63}$$

The loading of the shell is applied at the lower edge ($x = 0$). With the introduction of a load factor λ, the nondimensional applied load is given by

$$\bar{N}^{(0)} = \lambda \times N^{(0)}/N_{cl} \tag{64}$$

$$\bar{K}^{(0)} = \lambda \times K^{(0)}/N_{cl} \tag{65}$$

A computer program is developed, based on the preceding theory, called TASHA.

Table 4 Limit load factor by TASHA for A8 shell

N	Wave number set $\mathbb{N}$	Limit load factor λ_{lim}
1	{20}	0.26177
2	{20, 40}	0.344651
3	{20, 40, 60}	0.310071
4	{20, 40, 60, 80}	0.3099442
5	{20, 40, 60, 80, 100}	0.3099295

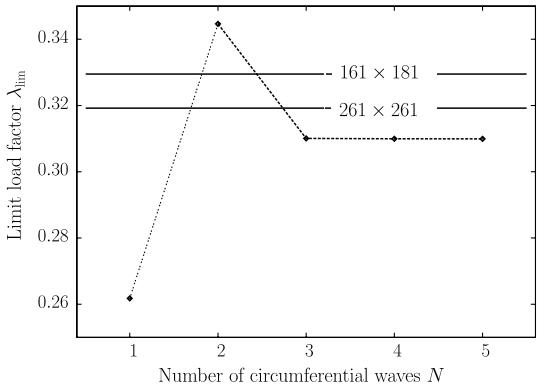

Fig. 7 Limit load factor λ_{lim}, for two STAGS-A models (solid line) and the values found using TASHA (dotted line) with various numbers of circumferential modes.

Numerical Example

The present theory is compared with a well-known program such as STAGS. The STAGS-A code at the Delft University of Technology is based on the finite difference method and is extensively modified by Brogran to give the most accurate results possible [8,9]. The isotropic Caltech A8 shell loaded by axial compression [10] is used for the comparison, the shell properties are shown in Table 2.

The boundary conditions of the shell edges are SS-3, the axial uniform compressive load is applied at the lower edge as follows:

$$\bar{N}_x(0) = -1.0 \times \lambda \qquad \bar{u}_{c,k}(0) = \bar{u}_{s,k}(0) = 0 \quad \text{for } k = 1, \cdots, N$$

The initial imperfection is given by

$$\bar{w}^* = \frac{w^*}{t} = 0.6882 \sin 17\pi \frac{x}{L} \cos 20 \frac{y}{R} \tag{66}$$

With the STAGS program the problem was solved with two different mesh sizes. The limit load factor λ_{lim} was computed. The results are shown in Table 3.

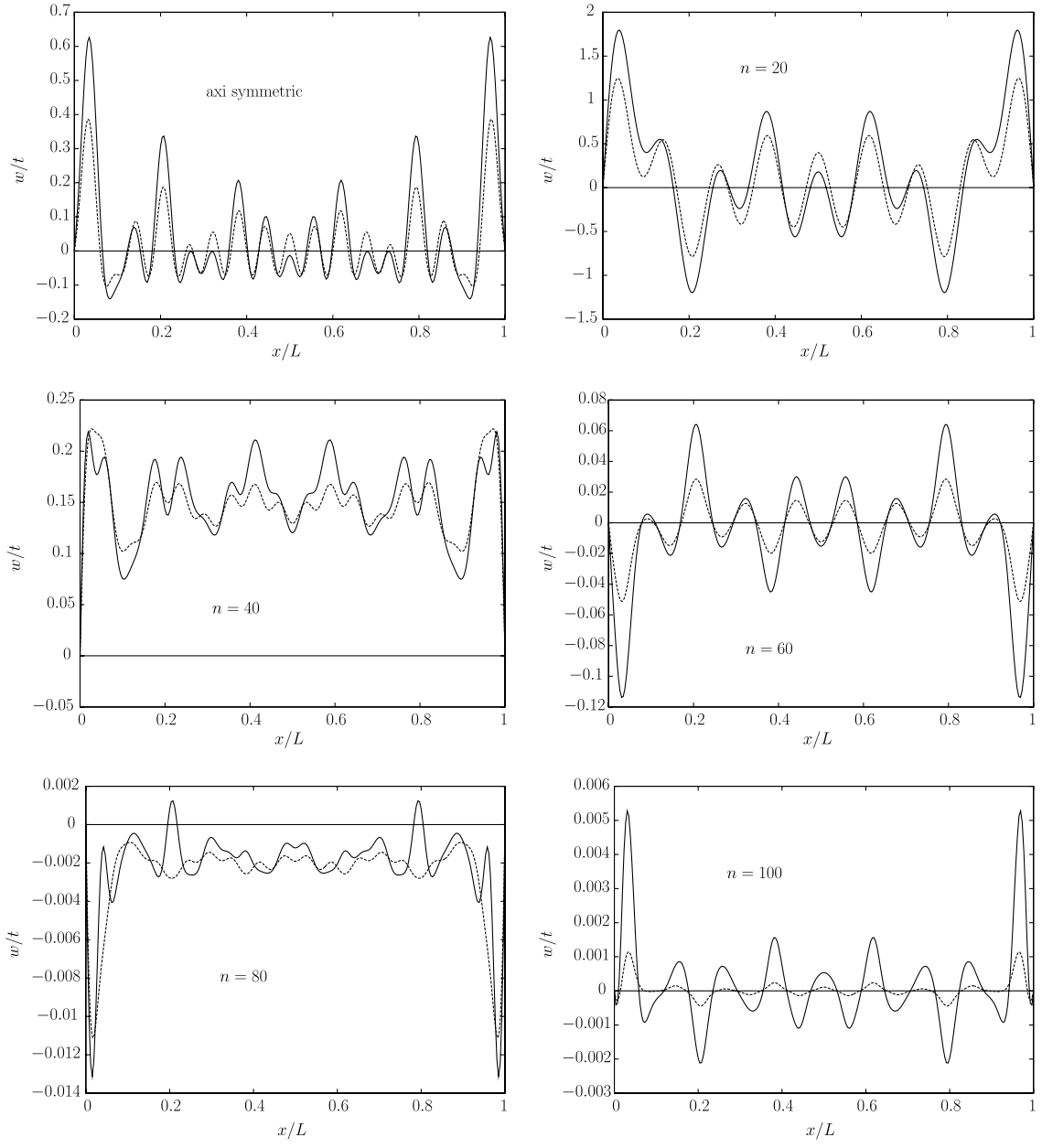

Fig. 8 Comparison of the radial displacement components obtained by STAGS 261 × 261 mesh (solid line) and current theory with $N = 5$ (dotted line).

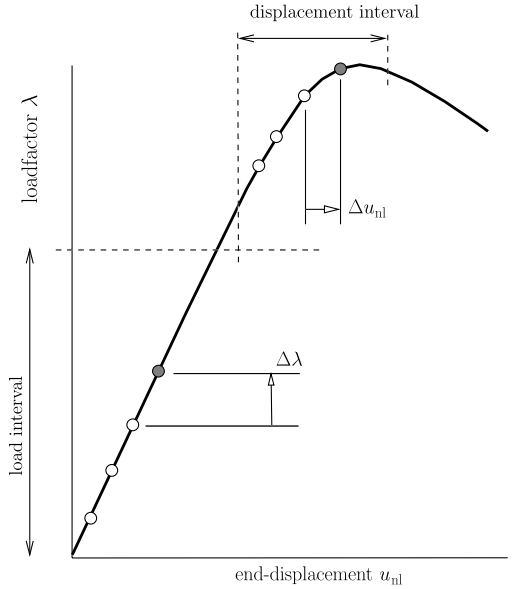

Fig. 9 Load-end displacement curve.

The radial displacements computed by STAGS at limit load was analyzed further. At each axial coordinate x, the Fourier series of the radial displacement was determined. The Fourier series is given by

$$[w(y)]_x \approx w_0 + \sum_{\ell=1}^{N_\ell}\left(w_{c,\ell}\cos\ell\frac{y}{R} + w_{s,\ell}\sin\ell\frac{y}{R}\right) \qquad (67)$$

For the course mesh with 181 points in circumferential direction the upper limit value $N_\ell = 80$, while for the finer mesh $N_\ell = 120$. The maximum and minimum values of the coefficients are shown in Fig. 6. Notice that the nonzero coefficient values are: the axisymmetric and the values corresponding to circumferential wave numbers $\ell = 20, 40, 60, \cdots$. This corresponds to the expected mode coupling equation Eq. (52). Also the decline of amplitudes of the modes corresponding to the larger values of circumferential wave numbers is prominent.

Table 4 and Fig. 7, show the limit load factors computed by TASHA based on the presented equations. It is clear that both STAGS and TASHA converge with a finer mesh and a larger number of modes in the set $\mathbb{N}$. TASHA has almost converged using a set of three circumferential wave numbers. If the number of wave numbers is too small $N = 1$, the response computed by TASHA is bad. This is caused by the fact that the response is poorly described by the short truncated series. Figure 8, shows the radial displacement components as a function of the axial coordinate for the STAGS 261×261 model and the TASHA $N = 5$ model both at limit load. Notice that the different modes show a good similarity up to $n = 60$. The modes with $n = 80$ and $n = 100$, are showing less similarity. This may be caused by the fact that the mesh size in circumferential direction used in the STAGS model has too few points (degrees of freedom) to describe the high number of circumferential waves accurately.

Table 5 Nonlinear analysis scheme of A8 shell

Interval number	Interval	Step size
	Load interval	$\Delta\lambda$
i	$0.005\cdots0.250$	5×10^{-3}
ii	$0.251\cdots0.300$	1×10^{-3}
	Displacement interval	Δu_{nl}
iii	$0.1700\cdots0.2190$	1×10^{-3}
iv ($N=4$)	$0.2191\cdots0.2209$	1×10^{-4}
iv ($N=5$)	$0.2165\cdots0.2184$	1×10^{-4}

CPU Times

The CPU time required by TASHA depends upon the shell geometry, the number of modes and the number of subintervals. The number of nonlinear first-order differential equations depends directly on the number of modes. For the parallel shooting method to converge the number of subintervals used must be sufficiently large, if the number is too low the numerical method fails. Either the load increment $\Delta\lambda$ or the increment of the nonlinear part of the end-displacement Δu_{nl} can be prescribed, see Fig. 9. The later being the end-displacement minus the linear membrane end-displacement.

For the A8 shell, the interval $\bar{x} = [0, L/R]$ is divided into 22 or 32 subintervals and the tolerance for the integration methods is $\epsilon = 1.010^{-7}$. The computer used for the calculations is a desktop PC with an ASUS P4G8X board and an Intel Pentium 4 3.066 GHz processor with 1.0 GB RAM under MS Windows XP Professional. TASHA is written in FORTRAN F77 and compiled with the Compaq Visual Fortran Ver. 6.6 compiler.

The computations were done in four stages. In the first two stages, the axial load was prescribed, in the last two stages the nonlinear end-shortening was prescribed, see Table 5. In Table 6, the CPU time required for a single incremental load or displacement step is shown. The total CPU time for $N = 4$ using 22 or 32 subintervals is about equal and the solution is exactly similar. The CPU time for $N = 5$ with 32 subintervals required about 8.5 h, which is about twice the CPU time for $N = 4$. The CPU time required by STAGS-A is approximately 18 h for the 161×181 model.

Discussion

The program TASHA based on the Sanders equations and the parallel shooting method is used to compute the buckling load for several other shells [11] such as the Caltech's stringer stiffened shell AS-2, and Khot's glass–epoxy shell [3] both under axial compression, and the graphite–epoxy shells by Fuchs et al. [12] under bending load. The results are in good agreement with the results obtained by other programs.

For programs based on finite difference or finite elements, a convergence study is necessary [13]. For the method presented here, a study on the size of the truncated Fourier series is required. If the models become larger, the present method requires less CPU time than the finite difference or finite element methods.

Conclusions

The results obtained by the current theory shows that the response has a good similarity with the STAGS-A results, and can be used as a research tool in the DISDECO program as a transition between level 2 and level 3. Further the response in high circumferential wave numbers may be used as a indication of the mesh size used in STAGS.

Care must be taken that the set of full circumferential wave numbers $\mathbb{N}$, contains a sufficient large number of relevant wave numbers.

Table 6 CPU times per incremental load or displacement step and total CPU time, s

Modes N	Subintervals	CPU time, interval i	CPU time, interval ii	CPU time, interval iii	CPU time, interval iv	Total CPU time
3	22	39.1	31.6	46.9	——	5884
4	22	91.5	87.3	110.3	68.0	15,740
4	32	90.6	82.4	110.5	74.3	15,587
5	32	178.7	161.0	218.5	141.4	30,742

References

[1] Arbocz, J., and Starnes, J. H., "Hierarchical High-Fidelity Analysis Methodology for Buckling Critical Structures," *Journal of Aerospace Engineering*, Vol. 18, No. 3, July 2005, pp. 168–178. doi:10.1061/(ASCE)0893-1321(2005)18:3(168)

[2] Arbocz, J., Starnes, J. H., and Nemeth, M. P., "Hierarchical Approach to Buckling Load Calculations," NASA Center for Aerospace Information, AIAA Paper 99-1232, 1999.

[3] Arobcz, J., de Vries, J., and Hol, J. M. A. M., "On the Buckling of Imperfect Anisotropic Shells with Elastic Edge Supports Under Combined Loading, Part 1: Theory and Numerical Analysis," Memorandum M-849, Delft Univ. of Technology, Dept. of Aerospace Engineering, Delft, The Netherlands, Sept. 1998.

[4] Sanders, J. L. Jr., "Nonlinear Theories for Thin Shells," *Quarterly Journal of Applied Mathematics*, Vol. 21, No. 1, 1963, pp. 21–36.

[5] Almroth, B. O., Brogan, F. A., Miller, E., Zele, F., and Peterson, H. T., "Collapse Analysis for Shells of General Shape: User's Manual for the STAGS-A Computer Code," Air Force Flight Dynamics Laboratory TR AFFDL-TR-71-8, Wright–Patterson Air Force Base, Ohio, March 1973.

[6] Rebel, G., "Nonlinear Theories for Imperfect Thin Shells," Delft Univ. of Technology, Dept. of Aerospace Engineering, Delft, The Netherlands, Rept. LR-750, Dec. 1993.

[7] Keller, H. B., *Numerical Methods for Two-Point Boundary Value Problems*, Dover, New York, 1992, par. 2.4, pp. 61–68.

[8] Arbocz, J., "The Effect of Imperfect Boundary Conditions on the Collapse Behaviour of Anisotropic Shells," *International Journal of Solids and Structures*, Vol. 37, Nos. 46–47 (W. T. Koiter Commemorative Issue), Nov. 2000, pp. 6891–6915. doi:10.1016/S0020-7683(99)00319-4

[9] Hol, J. M. A. M., "Improved Reliability of Buckling Load Calculations Using Multi-Level High-Fidelity Analysis," 47th AIAA/ASME/ASCE/AHS/ASC Structures, Structural Dynamics, and Material Conference, AIAA Paper 2006-2029, May 2006.

[10] Arbocz, J., and Babcock, C. D. Jr., "Experimental Investigation of the Effect of General Imperfections on the Buckling of Cylindrical Shells," NASA CR-1163, Sept. 1968.

[11] Notenboom, R. P., "Nonlinear Mode Interaction for Thin Imperfect Anisotropic Circular Cylindrical Shells Under Different Loading Conditions," Ph.D. Thesis, Delft Univ. of Technology, Dept. of Aerospace Engineering, Delft, The Netherlands, Dec. 2006.

[12] Fuchs, J. P., Hyer, M. W., and Starnes, J. H., Jr., "Numerical and Experimental Investigation of the Bending Response of Thin-Walled Composite Cylinders," Virginia Tech Center for Composite Materials and Structures, Blacksburg, VA, Rept. CCMS-93-19 and VPI-E-93-11, Sept. 1993; also NASA CR-195730.

[13] McNeal, R. H., *Finite Elements: Their Design and Performance*, Marcel Dekker, New York, 1994, pp. 71–99.

S. Pellegrino
Associate Editor